

A MODEL-BASED OPTIMAL OPERATION STRATEGY FOR COMPRESSED AIR ENERGY STORAGE (CAES) PLANTS

Fernando De Samaniego Steta, Andreas Ulbig¹, Stephan Koch, Göran Andersson
ETH Zurich

Power Systems Laboratory
Zurich, Switzerland

Email: fdesaman@student.ethz.ch, {ulbig, koch, andersson}@eeh.ee.ethz.ch

Abstract - A model-based optimal operation strategy for an energy storage system exhibiting significant stand-by energy losses is presented. Specifically, a thermodynamic model of an advanced adiabatic compressed air energy storage (AA-CAES) plant, consisting of compression/expansion trains, a thermal energy storage (TES) system, and an underground cavern for compressed air storage, is used in this work. An operation strategy based on this model is proposed for the commercial operation of CAES systems and other storage systems exhibiting stand-by losses within existing power market regimes. A multi-objective, multi-period optimization problem is formulated and solved within a model predictive control (MPC) scheme, using electricity spot prices from the European Power Exchange (EPEX).

Keywords - Lossy Energy Storage, Compressed Air Energy Storage (CAES), AA-CAES, Multi-Objective Optimization, Model Predictive Control (MPC)

1 Introduction

THE large-scale deployment of fluctuating renewable energy sources (RES) in recent years, notably in the form of wind turbines and PV installations, significantly increases the share of stochastic and as such non-controlled power production in the electric power systems of many countries [1]. As this trend is expected to continue in coming years, it will become increasingly difficult to manage and allocate the stochastic power in-feed in day-to-day power system operation [2]. This has generated an interest in large-scale energy storage systems, as the additional storage capacity would increase the flexibility in power system operation for aligning the stochastic processes of fluctuating renewable energy generation and electricity demand. For the time being, pumped hydro storage (PHS) and compressed air energy storage (CAES) are the only technologies available that can provide sufficiently storage capacities [3]. CAES technology in particular has regained attention in the last decade due to its similar investment costs and less geographic restrictions when compared to PHS systems [4]. The functional principle of CAES technology is to store surplus electric energy in the form of mechanical energy by compressing air into an underground reservoir. The electric energy can be regained by expanding the air in a gas turbine. Currently, there are two CAES storage plants in operation worldwide, one in Huntorf, Germany (commissioned in

1978, 321 MW, 640 MWh, $\eta \approx 40\%$) and one in McIntosh, USA (commissioned in 1991, 110 MW, 2860 MWh, $\eta \approx 54\%$) [5, 6]. Different CAES concepts have been developed. Under the premises of a future low-carbon energy system, the most attractive option is the advanced adiabatic compressed air energy storage (AA-CAES) system due to its higher storage cycling efficiency. In this concept, the heat energy expelled during the compression stage is recovered and stored in a thermal energy storage, and later used for re-heating the stored compressed air that goes into the expansion stage, eliminating the pre-heating combustor needed in the original CAES concept [7]. The round-trip efficiency of an AA-CAES depends primarily on the energy losses of the thermal energy storage and is in the range of 50–75% [7–10].

The thermal energy storage (TES) system of an AA-CAES plant inherently suffers time-dependent heat energy losses as a result of inevitable heat exchanges with its surroundings, therefore making it a lossy energy storage unit. Another significant albeit less important heat sink in the plant is the underground cavern used for storing the compressed air. Due to the heat losses incurred during plant idle time, the nominal turbine inlet temperature cannot be maintained over the whole discharging time after extended storage periods. This decreases the air pressure difference while expanding, thus progressively reducing the plant's electric output over the discharging time. (See Figure 2 later in this article.) Hence, both the plant's electric output as well as its round-trip efficiency depend on the storage time. In this context, a newly developed model of an AA-CAES plant that captures the described dynamic effects is presented. The model was built using MATLAB's Simulink environment. Considerable research work on CAES modeling has been accomplished by several research groups in recent years [11–13]. If AA-CAES systems are to be widely deployed, they will have to operate within existing power market regimes. Like PHS systems, they need to be able to take advantage of price arbitrage opportunities from the daily fluctuation of spot market prices. In the case of AA-CAES systems, the non-negligible time-dependent energy losses have to be considered additionally, which is the main motivation for developing an operation strategy specifically for AA-CAES plants. The optimization is implemented within a model predictive control (MPC) scheme, which uses linearized models of the original nonlinear AA-CAES plant

¹corresponding author

model, while respecting *a priori* defined operational limits of the plant, i.e. power and energy constraints. The optimization setup is multi-objective due to the two competing objectives of maximizing profit from spot price arbitrage while reducing the system's time-dependent energy losses. The optimization has to be multi-period since storage optimization is an inter-temporal task. All simulations were run using hourly-based spot price profiles from the European Power Exchange (EPEX) [14].

The remainder of this paper is organized as follows: Section 2 addresses the construction of the thermodynamic AA-CAES model, describing each component of the model and its operation states. Section 3 presents the formulation and implementation of the proposed multi-objective, multi-period optimal operation strategy for the AA-CAES model, discussing the parameters and linearizations used. Section 4 presents simulation results obtained from the modeling and optimization work of the former sections. Finally, Section 5 discusses the results and concludes with an outlook on further research work.

2 Modeling of an AA-CAES plant

The AA-CAES plant model consists of four main modules, representing electric energy input and output trains as well as two energy storage units for heat and mechanical energy. Each module contains a model for the respective main physical processes including the occurring energy losses. The first module considers a 64 MW compressor train (CT) and models the extraction of the heat expelled in the compression stage. The second and third modules represent the thermal energy storage (TES) and the mechanical energy storage (cavern), respectively. The fourth module describes the air re-heating and expansion stage through an 85 MW expansion train (ET). Compression and expansion trains have heat exchangers (HX) for transferring heat between the air and a heat transfer fluid. The plant's nominal round-trip efficiency is $\eta_{AA-CAES} = 57\%$ (not including idle losses from extended storage time).

Figure 1 shows a diagram of the AA-CAES model, where the inputs are atmospheric air and electric power to drive the compressor train ($\dot{E}_{elec,c}$). The terms $\dot{m}_{air,c}$ and $\dot{m}_{air,t}$ correspond to the air mass flows of the compressor and expansion trains, respectively. Energy dissipation ($\dot{E}_{loss,cav}$ and $\dot{E}_{loss,TES}$) occurs at the cavern walls and between the TES and the environment.

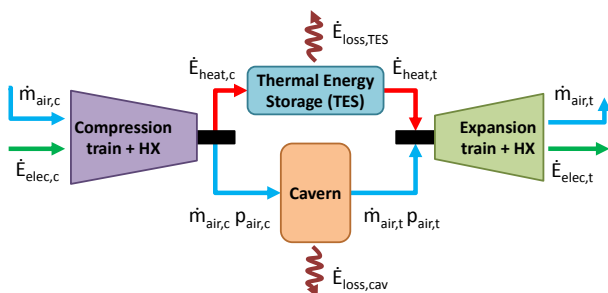


Figure 1: Diagram of an AA-CAES model (HX: Heat Exchanger).

The model considers air to be an ideal binary gas with constant specific heat capacities ($c_p/c_v = 1.4$). After the compression stage, the air is stored in an underground salt cavern having a volume of $V_{sc} = 560,000 \text{ m}^3$. A salt cavern was chosen due to the relative abundance of favorable geologic formations and comparably low costs [4]. A cylindrical sensible heat TES system made of high temperature concrete was chosen due to its low capital and maintenance costs [15]. Each HX has an efficiency of $\eta_{HX} = 70\%$, using oil as a heat transfer fluid (HTF) for charging/discharging the TES system. Possible leakage of air in the cavern or oil in the TES/HX is neglected. The CT compressors have an efficiency of $\eta_c = 88\%$ and operate with a constant air mass flow of $\dot{m}_{air,c} = 120 \text{ kg/s}$ and a compression ratio of $\beta_{CT} = 65$ when in use. The ET turbines have an efficiency of $\eta_t = 80\%$, a mass flow of $\dot{m}_{air,t} = 240 \text{ kg/s}$ and an expansion ratio of $\beta_{ET} = 46$. Compression/expansion ratios were chosen in accordance with the salt cavern's minimum/maximum pressure limits.

The AA-CAES model has three different operation states: air compression, air expansion and idle. The last state represents the situation where neither compression nor expansion is taking place. In the compression state, electricity is consumed for compressing air into the cavern, while the recovered heat is sent to the TES. In the expansion state heat and air are withdrawn from the TES and the cavern, respectively, to produce electricity in the expansion train. Due to the given air mass flows, compression and expansion operation stages need 23 hours to fully charge and 11 hours to fully discharge the plant. The state-of-charge (SOC) of the AA-CAES plant as well as the mass of air contained in the salt cavern vary over time according to the evolution of the operation states. The salt cavern's air mass is governed by

$$\frac{dm_{air}}{dt} = \dot{m}_{air,c} - \dot{m}_{air,t} , \quad (1)$$

stating that the total mass of the air in the cavern is determined by the difference between air mass in- and outflow. These mass flows are set by the compression and expansion states, respectively. The temperature of the TES system is given by the first-order differential equation

$$(\rho \cdot V \cdot c_p)_{TES} \frac{dT_{TES}}{dt} = \dot{E}_{heat,c} - \dot{E}_{heat,t} - \dot{E}_{losses} , \quad (2)$$

in which $\dot{E}_{heat,c}$ is the heat injected to the TES during compression, $\dot{E}_{heat,t}$ is the heat withdrawn from the TES during expansion, and $\dot{E}_{losses} = \dot{E}_{loss,cav} + \dot{E}_{loss,TES}$ refers to heat energy dissipation from the TES system and the salt cavern. Air temperature inside the cavern (T_{cav}) is described by the first-order differential equation

$$\frac{dT_{cav}}{dt} = \left(\frac{dT_{cav}}{dt} \right)_{adiabatic} + \left(\frac{dT_{cav}}{dt} \right)_{isobaric} , \quad (3)$$

where the adiabatic term is the result of the change in air pressure over time in the compression or expansion state, while the isobaric term considers the heat transfer between

the cavern's wall and the compressed air. Solving this latter term requires the knowledge of the cavern's wall temperature ($T_{cav,w}$) at every time step t , which is described by stationary heat conduction. This physical process is represented by *Fourier's Equation* for constant heat conduction coefficients without a heat source. For the case of a cylindrical semi-infinite cavern it is given as

$$\frac{\partial T_{cav,w}}{\partial t} = r_{diff} \left(\frac{\partial^2 T_{cav,w}}{\partial r^2} + \frac{1}{r} \frac{\partial T_{cav,w}}{\partial r} \right), \quad (4)$$

where r_{diff} is the diffusivity (m^2/s), which depends on the cavern wall's properties [16], and r is a distance measured from the cavern's wall to a point inside the rock. Equation (4) can be solved by using the *Finite Differences Method* for discretizing the space derivatives in order to arrive at a differential equation that solely depends on time. This can easily be integrated in MATLAB/Simulink. Once $T_{cav,w}$ is known, (3) can be solved. The heat losses considered in (3–4) model the time-dependence of the AA-CAES plant's electric output. They account for the reduction of the system's SOC as a function of the storage time, thus capturing the storage unit's energy stand-by losses. Figure 2 shows the plant's absolute and relative energy losses (top and middle) together with the decrease in efficiency (bottom) as a function of the idle time duration.

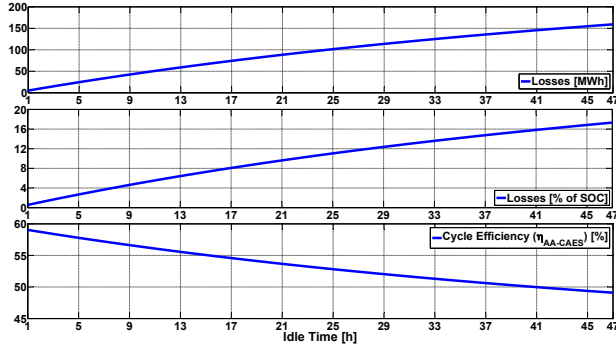


Figure 2: Evolution of occurring energy losses (top) and the AA-CAES plant's efficiency during idle time.

As shown in Figure 2, the energy losses are around 10% per day of the initial SOC. Hence, the losses are equivalent to around 5–10% of the total energy storage capacity while fully discharging (11 h) or charging (23 h) the AA-CAES plant. The inherent energy losses of the plant are thus not negligible but need to be taken into account when calculating an optimal operation strategy.

To sum up the section, the AA-CAES plant model depends on four differential equations in time, which can be solved for each time step t using the integrator function of MATLAB/Simulink (variable-step solver ODE45 Dormand–Prince). The results presented here provide a first insight of the plant's performance when time-dependent energy losses are considered. The above given model can be used to analyze the possible power system applications of AA-CAES plants, e.g. price arbitrage and ancillary services.

3 Calculating a model-based operation strategy

The optimal operation strategy for the AA-CAES plant is formulated as a model predictive control (MPC) scheme using the previously derived AA-CAES plant model. The MPC scheme is implemented using the freely available YALMIP toolbox [17] for MATLAB in combination with the general purpose solver `fmincon` [18].

3.1 MPC Optimization Setup

A multi-period optimization is implemented in the following manner: The optimization setup is defined in the same form as for a standard linear or quadratic optimization problem. However, the cost function is defined for the whole finite prediction horizon $T_p = N \cdot T_s$. For brevity, T_s is dropped from subsequent notation, i.e. the prediction horizon becomes $[t, t+T_p] = [t, t+N]$. The internal plant model given to the MPC scheme is used for predicting the evolution of the system state vectors $\hat{\mathbf{x}}(t+1, \dots, t+N | t)$ over the *a priori* defined prediction horizon². An actual plant state measurement $\mathbf{x}(t)$ is used for calculating possible state evolution paths as a function of an optimal control input strategy $\mathbf{u}^*(t, \dots, t+N)$ until the end of the horizon. The first input vector $\mathbf{u}^*(t)$ is then implemented and the whole MPC scheme is updated with the newly measured plant state vector $\mathbf{x}(t+1)$ [19]. System state and control input constraints can be defined explicitly.

As the system dynamics of the AA-CAES plant model are governed by four differential equations, state-space linearization is straightforward. A discrete-time state-space representation of the AA-CAES model is used for predicting the plant's system state \mathbf{x} over an hourly-based prediction horizon T_p . Using linear state-space models has the advantages of easy generalization of multi-variable systems, ease of analysis of closed-loop properties, and reduced computational effort [20]. Two optimal operation strategies are established using either linear-time invariant (LTI) or piece-wise affine (PWA) discrete-time models.

A discrete-time linear time-invariant (LTI) system is described in state-space form by the expressions

$$\begin{aligned} \mathbf{x}(t+1) &= \mathbf{A} \mathbf{x}(t) + \mathbf{B} \mathbf{u}(t) \\ \mathbf{y}(t) &= \mathbf{C} \mathbf{x}(t) + \mathbf{D} \mathbf{u}(t), \end{aligned} \quad (5)$$

where $\mathbf{x} \in \mathbb{R}^n$ is the discrete system state vector, $\mathbf{u} \in \mathbb{R}^m$ the discrete control input vector and $\mathbf{y} \in \mathbb{R}^l$ the discrete system output. The system matrix is given as $\mathbf{A} \in \mathbb{R}^{n \times n}$ and the control input matrix as $\mathbf{B} \in \mathbb{R}^{n \times m}$. The output equation is given by the matrices $\mathbf{C} \in \mathbb{R}^{l \times n}$ and $\mathbf{D} \in \mathbb{R}^{l \times m}$. The initial state vector of the system is $\mathbf{x}(0) = [x_1(0), \dots, x_n(0)]^T = \mathbf{x}_0$. The constraints on system state \mathbf{x} , system output \mathbf{y} and control input \mathbf{u} , see Eq. (5), are given in the form of compact polyhedral sets

$$\mathbf{x} \in \mathbb{X} \in \mathbb{R}^n, \quad \mathbf{y} \in \mathbb{Y} \in \mathbb{R}^l, \quad \mathbf{u} \in \mathbb{U} \in \mathbb{R}^m, \quad (6)$$

which contain the origin in their interior.

LTI systems can easily be extended to PWA systems, which are able to model non-linear and non-smooth processes [21]. A set of three inter-connected PWA linear

²The notation indicates the predicted evolution system state $\hat{\mathbf{x}}(t+1, \dots, t+N)$, calculated at time instant t using the measured system state $\mathbf{x}(t)$.

models, one for approximately modeling each of the three operation states of the AA-CAES plant (compression, expansion and idle), can be defined as MPC-internal model. A general discrete-time PWA system is given by

$$\begin{aligned} \mathbf{x}(t+1) &= \mathbf{A}_i \mathbf{x}(t) + \mathbf{B}_i \mathbf{u}(t) + \mathbf{f}_i \\ \mathbf{y}(t) &= \mathbf{C}_i \mathbf{x}(t) + \mathbf{D}_i \mathbf{u}(t) + \mathbf{g}_i \\ \forall \begin{bmatrix} \mathbf{x}(t) \\ \mathbf{u}(t) \end{bmatrix} &\in \Omega_i, \end{aligned} \quad (7)$$

where the convex polyhedra $\Omega_i \subset \Omega \in \mathbb{R}^{n+m}$ are defined by a finite number of linear inequalities for the inputs and states of the system. The vectors \mathbf{x} , \mathbf{y} , \mathbf{u} and matrices \mathbf{A} , \mathbf{B} , \mathbf{C} , \mathbf{D} have the same dimensions as in the case of an LTI system. The index $i \in I = \{1, \dots, d\} \subset \mathbb{N}$ represents the possible dynamics of the linear system, where d is the total of all plant dynamics. The first term in Equation (7) together with its restrictions, is abbreviated as $\mathbf{x}(t+1) = f_{PWA}(\mathbf{x}(t), \mathbf{u}(t))$.

In order to regulate an LTI or a PWA system while respecting any imposed constraints (Eq. 6), the following cost function needs to be introduced:

$$\begin{aligned} J(\mathbf{u}, \mathbf{x}_0) &= L_N(\mathbf{x}(t+N)) + \sum_{k=t}^{t+(N-1)} L_k(\mathbf{x}(k), \mathbf{u}(k)) \\ &= \|\mathbf{Q}_f \mathbf{x}(t+N)\|_l + \sum_{k=t}^{t+(N-1)} (\|\mathbf{Q} \mathbf{x}(k)\|_l + \|\mathbf{R} \delta \mathbf{u}(k)\|_l), \end{aligned} \quad (8)$$

where $L_k \in \mathbb{R}^{n \times m}$ represents the so-called stage cost and $L_N \in \mathbb{R}^{n \times m}$ the so-called terminal state cost. The objective function can be linear or quadratic by choosing $l \in \{1, \infty\}$ or $l = 2$, respectively. The matrices \mathbf{Q} and \mathbf{R} define the cost terms for the system state $\mathbf{x}(t)$ and the control input $\mathbf{u}(t)$, respectively. \mathbf{Q}_f is a terminal system state constraint. Obtaining optimal control moves over the given prediction horizon N is then equivalent to solving the constrained finite-time optimal control (CFTOC) problem for an LTI or PWA system

$$\mathbf{u}^*(\mathbf{x}_0) = \arg \min_{\mathbf{u}(\cdot)} J(\mathbf{u}, \mathbf{x}_0) \quad (9)$$

$$s.t. \begin{cases} \mathbf{x}_0 = \mathbf{x}(0) \\ \mathbf{x}(t+1) = \mathbf{A} \mathbf{x}(t) + \mathbf{B} \mathbf{u}(t) \quad (\text{LTI}) \\ \mathbf{x}_0 = \mathbf{x}(0) \\ \mathbf{x}(t+1) = f_{PWA}(\mathbf{x}(t), \mathbf{u}(t)) \\ \forall [\mathbf{x}(t), \mathbf{u}(t)]^T \in \Omega \quad (\text{PWA}) \end{cases}$$

$$\mathbf{x} \in \mathbb{X} \in \mathbb{R}^n, \quad \mathbf{y} \in \mathbb{Y} \in \mathbb{R}^n, \quad \mathbf{u} \in \mathbb{U} \in \mathbb{R}^m$$

$$\begin{cases} \mathbf{Q} = \mathbf{Q}^\backslash \succeq 0, \mathbf{Q}_f = \mathbf{Q}_f^\backslash \succeq 0, \mathbf{R} = \mathbf{R}^\backslash \succeq 0, \text{ if } l = 2 \\ \text{rank}(\mathbf{Q}) = n, \text{rank}(\mathbf{R}) = m, \text{ if } l \in \{1, \infty\}. \end{cases}$$

The hereby derived optimal control input is given by $\mathbf{u}^*(\mathbf{x}_0) \equiv [\mathbf{u}(t), \dots, \mathbf{u}(t+N)]^T \in \mathbb{R}^{m \times N}$.

3.2 MPC-internal Model of the AA-CAES Plant

Within the different modules of the AA-CAES model, there are altogether four main variables that represent the dynamic system states. Each entry of the state vector $\mathbf{x}(t)$ contains a variable from each of the differential equations of the model, Eqs. (1–4). The state vector is thus given by

$$\mathbf{x}(t) = [T_{\text{cav}}(t), T_{\text{TES}}(t), m_{\text{air}}(t), T_{\text{cav,w}}(t)]^T, \quad (10)$$

including the cavern temperature $T_{\text{cav}}(t)$, the thermal energy storage temperature $T_{\text{TES}}(t)$, the cavern air mass $m_{\text{air}}(t)$ and the cavern wall temperature $T_{\text{cav,w}}(t)$. The system state $\mathbf{x}(t)$ is the same in LTI and PWA models.

The control input variable $\mathbf{u}(t) \in \mathbb{R}^2$ determines the operation state of the plant, where $u_1(t)$, $u_2(t)$ correspond to the compression and expansion states, respectively. As $u_i(t) \in [0, 1] \forall i$, the plant's idle state is described by both entries being equal to zero, i.e. no compression and no expansion. The control input is restricted to only one operation state at a time. This renders the optimization problem mixed-integer, thus numerically more demanding.

As the system vector $\mathbf{x}(t)$ of the model is fully observable, i.e. measurable, Eq. (5) can be re-written as

$$\begin{aligned} \mathbf{x}(t+1) &= \mathbf{A} \mathbf{x}(t) + \mathbf{B} \mathbf{u}(t), \\ \mathbf{y}(t) &= [\mathbf{x}^T(t), P_{\text{cav}}(t)]^T, \end{aligned} \quad (11)$$

where the cavern pressure, $y_5(t) = P_{\text{cav}}(t)$, is introduced as an additional observable state in the output vector \mathbf{y} . The cavern pressure is directly dependent on some of the system states and is constructed, using the ideal gas law, as $P_{\text{cav}}(t) = \frac{R_{\text{air}}}{V_{\text{cav}}} \cdot T_{\text{cav}}(t) \cdot m_{\text{air}}(t) = \frac{R_{\text{air}}}{V_{\text{cav}}} \cdot x_1(t) \cdot x_3(t)$, with R_{air} being the specific gas constant of air. The term is linearised for the boundary values of $x_1(t) = T_{\text{cav}}(t)$, e.g. $P_{\text{cav}}^{\text{min/max}}(t) = \left[\frac{R_{\text{air}}}{V_{\text{cav}}} \cdot T_{\text{cav}}^{\text{min/max}} \right] \cdot m_{\text{air}}(t)$.

For the case of LTI models, the system is given as

$$\mathbf{A} = \begin{pmatrix} 0.969 & 0 & 5.16 \times 10^{-9} & 0.030 \\ 0 & 0.994 & 0 & 0 \\ 0 & 0 & 1 & 0 \\ 0.007 & 0 & 1.89 \times 10^{-11} & 0.939 \end{pmatrix}, \quad (12)$$

$$\mathbf{B} = \begin{pmatrix} 1.225 & -2.048 \\ 11.090 & -4.277 \\ 4.320 \times 10^5 & -8.640 \times 10^5 \\ 0.005 & -0.008 \end{pmatrix}. \quad (13)$$

The plant's constraints limit the system's output vector \mathbf{y} according to the minimum and maximum values allowed in the AA-CAES model. They are selected as

$$\begin{aligned} 293.0 \text{ K} &\leq y_1(t) = x_1(t) \leq 312.6 \text{ K}, \\ 432.6 \text{ K} &\leq y_2(t) = x_2(t) \leq 502.8 \text{ K}, \\ 3 \times 10^7 \text{ kg} &\leq y_3(t) = x_3(t) \leq 4.1 \times 10^7 \text{ kg}, \\ 293.0 \text{ K} &\leq y_4(t) = x_4(t) \leq 293.65 \text{ K}, \\ 46.0 \text{ bar} &\leq y_5^{\text{min}}(t) = P_{\text{cav}}^{\text{min}}(t), \\ &y_5^{\text{max}}(t) = P_{\text{cav}}^{\text{max}}(t) \leq 65.0 \text{ bar}. \end{aligned} \quad (14)$$

For the optimization problem definition, only a cost function for the inputs $\mathbf{u}(t)$ was considered. It is given by

$$R(t) = Q(t) \cdot (\mathbf{E}_{\text{cost}} \cdot \mathbf{w}(t)) , \quad (15)$$

where $R(t)$ is the total revenue of the plant at time step t , measured in Euros. The term $Q(t)$ is a scalar that represents the electricity price at time step t . The vector $\mathbf{w}(t)$ is constructed using the input vector $\mathbf{u}(t)$ and is given by

$$\mathbf{w}(t) = [u_1(t), u_2(t), (u_1(t) - 1) \cdot (u_2(t) - 1)]^T , \quad (16)$$

where the third entry $w_3(t) = 0$, whenever the plant is either in full compression or expansion state. The third entry $w_3(t) = 1$, whenever the plant is in idle state, i.e. $u_1(t) = u_2(t) = 0$. The vector $\mathbf{w}(t)$ is constrained in the same way as $\mathbf{u}(t)$, meaning that only one entry can be different from zero in each time step. The term $\mathbf{w}(t)$ renders the cost function (15) mixed-integer.

In Eq. 15, the term \mathbf{E}_{cost} is a constant vector that considers the hourly electricity production or consumption by the AA-CAES plant for each operation state:

$$\mathbf{E}_{\text{cost}} = [-64 \text{ MWh}, 85 \text{ MWh}, -3 \text{ MWh}] , \quad (17)$$

where the first two entries are the nominal electric energy values consumed by the compression train or produced by the expansion trains, while the third entry corresponds to the electric energy lost while in idle state (all values are given for a duration of one hour). Energy production and consumption are represented by positive and negative signs, respectively.

The structure of the optimization scheme is as follows: An operation strategy $\mathbf{u}(t, \dots, t + N | t)$ is calculated via the described MPC scheme and based on the measured system state $\mathbf{x}(t)$. Only the first step $\mathbf{u}(t)$ is passed on as control input to the non-linear AA-CAES model in MATLAB/Simulink. The resulting plant system state $\mathbf{x}(t + 1)$, is then given to the MPC scheme as control feedback and used for the calculation of the updated operation strategy $\mathbf{u}(t + 1, \dots, (t + 1) + N | t + 1)$. The initial system state $\mathbf{x}(0)$, which also defines the state-of-charge (SOC) of the AA-CAES plant, is needed for the first time step t_0 . The thus resulting optimal operation strategy \mathbf{u} dictates the operating state of the AA-CAES plant, i.e. compression, expansion or idle, for the next time step $t + 1$.

The employed electricity spot price time-series are real price profiles obtained from the European Power Exchange (EPEX) spot market [14]. The price profiles are assumed to be perfectly predictable up to the end of the MPC scheme's prediction horizon $T_p = N \cdot T_s = N \cdot 1 \text{ h}$. Note that, although this is an idealistic assumption, in practice sufficiently accurate spot-price prediction tools exist. Furthermore, it is straightforward to update the price prediction continuously within the MPC framework in the case of non-perfect predictions.

A multi-objective, multi-period optimization needs to be performed for the following reasons: First, the operation strategy maximizes the profit of the plant while at the same time minimizing the time-dependent energy losses.

Second, storage operation implies inter-temporal dependencies, for example on storage levels and other operation constraints, which need to be tackled via a multi-period optimization. Furthermore, the continuous prediction updates due to new incoming price information can be incorporated easily into the optimization scheme. The notion of a finite prediction horizon implies that only price information up to the end of this horizon is available for the optimization task and that this information will be continuously updated as the horizon moves forward. A diagram of the optimization setup is shown in Figure 3.

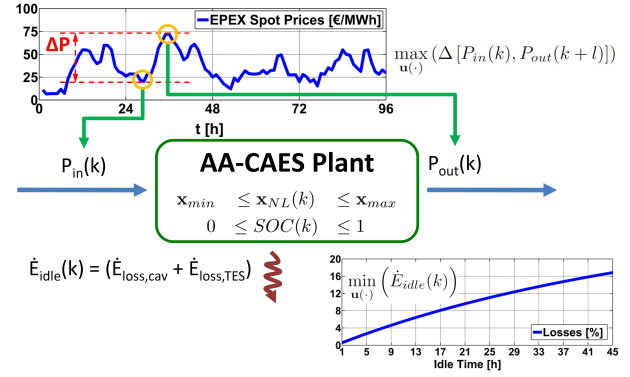


Figure 3: Objectives of the AA-CAES plant operation optimization.

In Figure 3, the state \mathbf{x}_{NL} refers to the state of the non-linear AA-CAES model, which is restricted according to the constraints given above. The terms $P_{in}(t)$ and $P_{out}(t)$ represent the electricity prices from which the plant profits at compression and expansion states, respectively. Thus, the MPC controller tries to maximize the price difference between charge and discharge hours, while minimizing the time-dependent energy losses of the storage at the same time. A sensitivity analysis over the optimization setup's prediction horizon T_p is depicted in Figure 4. The plant's revenue function, i.e. its operation performance index, was calculated for different prediction horizon lengths, $T_p = 2 \text{ h}, \dots, 72 \text{ h}$. As can be seen, the performance gained from increasing the prediction horizon, e.g. having more information about the future spot price developments, levels off once the prediction horizon T_p reaches a certain length N (here for $T_p \approx 14 \text{ h}$). This is in accordance with MPC theory.

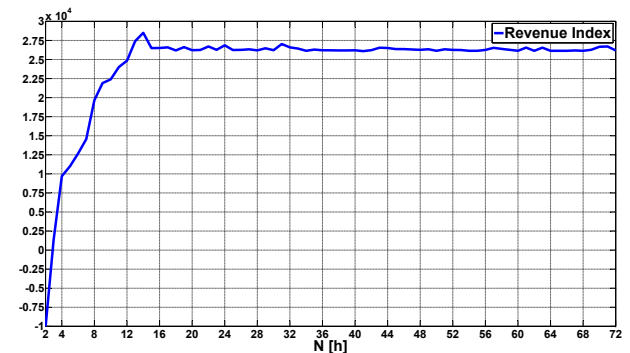


Figure 4: Revenue performance of the AA-CAES plant for different prediction horizon lengths ($T_p = 2 \text{ h} \dots 72 \text{ h}$, Simulation time: 7 days).

4 Simulation Results and Analysis

Operation performance of the presented optimal operation strategy was tested on spot price profiles from different years, for example including noteworthy events such as highly negative spot prices seen in some hours, using various prediction horizon lengths T_p . Figure 5 depicts a typical example of an optimal operation strategy calculated for a full week using spot price data of the first week of January 2007. For this calculation, the initial condition $\text{SOC} = 50\%$ and a prediction horizon of $T_p = 24$ h were employed. The figure presents the EPEX hourly electricity spot price-profile used for this particular optimization (top), the plant's optimal operation strategy (middle), where the absence of any bars at a given time corresponds to the idle operation state, while the blue and red bars correspond to the compression and expansion operation states, respectively. The plant's revenue at each time step of the operation strategy is given as well (bottom).

An impression of another simulation period, including an unusual price spike seen in the 4th week of January 2007, is presented in Figure 6. Additionally, the evolution of the plant parameters (T_{TES} , T_{cav} and p_{cav}) is depicted in Figure 7 for the same simulation period. Here, the prediction horizon length was chosen as $T_p = 24$ h while the initial state-of-charge is again $\text{SOC} = 50\%$. The plant dynamics for an extended idle operation state is illustrated in Figure 8. It presents the evolution over time of the variables involved in the model's energy losses and shows the physics behind the dynamic behavior, i.e. energy stand-by losses, already seen in Figure 2. An optimization run using the same parameters but capturing the whole month of January 2007 can be seen in the Annex (Figure 9).

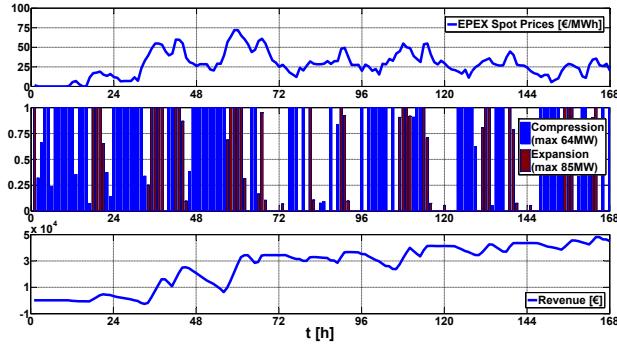


Figure 5: Optimal operation strategy of the AA-CAES model (Simulation time: 1–7 January 2007, $T_p = 24$ h, initial SOC: 50%).

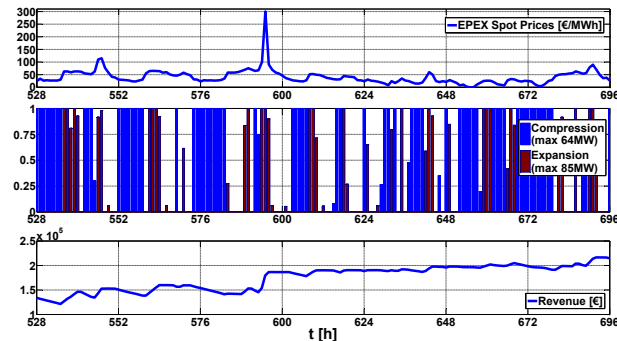


Figure 6: Optimal operation strategy of the AA-CAES model (Simulation time: 22–29 January 2007, $T_p = 24$ h, initial SOC: 50%).

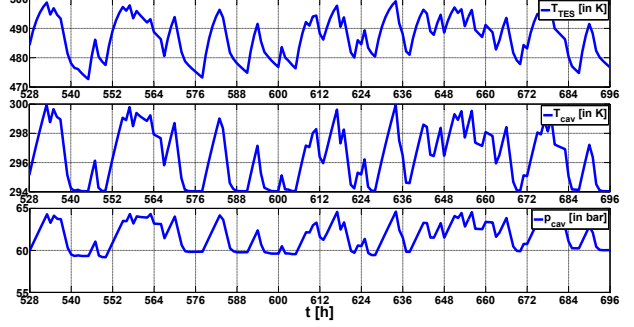


Figure 7: Evolution of AA-CAES plant parameters (Simulation time: 22–29 January 2007, $T_p = 24$ h, initial SOC: 50%).

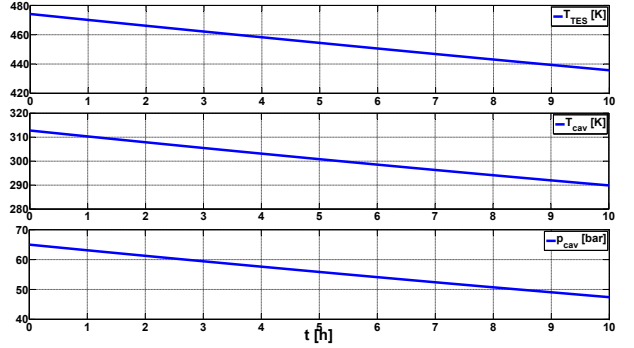


Figure 8: Evolution over time of air temperature (top), cavern pressure (middle) and TES output temperature (bottom).

5 Conclusion and Outlook

A thermodynamic model of an advanced adiabatic compressed air energy storage (AA-CAES) plant as well as a model-based optimal operation strategy were presented. The operation strategy has been derived via a multi-objective, multi-period optimization, using linearized plant models (LTI and PWA) as internal models of a model predictive control (MPC) scheme. The optimization setup and the obtained results are proposed as a performance benchmark for the integration of, in particular, AA-CAES storage plants into existing power market regimes. Here, AA-CAES storage plants constitute an example of lossy energy storage systems. Future research includes a detailed sensitivity analysis for varying optimization and plant dynamics parameters for both the LTI and PWA internal plant models. Furthermore, the applicability of the presented model-based predictive optimization scheme for a more generalized class of lossy energy storage systems will be investigated using the recently presented Power Nodes modeling framework [22].

Acknowledgments

The authors would like to thank Prof. Dr. Gianfranco Rizzo from the University of Salerno, Italy, for his valuable advice and information regarding CAES plant modeling. A model developed in his research group by Dr. Vincenzo Marano [11] has been a valuable reference for the modeling work presented in Section 2.

The EPEX electricity spot price data was kindly provided by the European Energy Exchange (EEX) [23].

REFERENCES

- [1] REN21. Renewables 2010 Global Status Report. www.ren21.net, 2010.
- [2] International Energy Agency (IEA). Harnessing Variable Renewables: A Guide to the Balancing Challenge. www.iea.org/w/bookshop/add.aspx?id=405, 2011.
- [3] H. Ibrahim, A. Ilinca, and J. Perron. Energy Storage Systems – Characteristics and Comparisons. *Renewable and Sustainable Energy Reviews*, 12(5):1221 – 1250, 2008.
- [4] S. Succar and R. H. Williams. Compressed Air Energy Storage: Theory, Resources and Applications for Wind Power. Technical report, Princeton, New Jersey, April 2008.
- [5] E.ON. Presentation of the Huntorf CAES Plant. www.kraftwerk-wilhelmshaven.com/pages/ekw_de/Huntorf/Uebersicht/index.htm, last retrieved 3 December 2010.
- [6] PowerSouth. Presentation of the McIntosh CAES Plant. www.powersouth.com/mcintosh_power_plant, last retrieved 3 December 2010.
- [7] C. Jakiel, S. Zunft, and A. Nowi. Adiabatic compressed air energy storage plants for efficient peak load power supply from wind energy: The European project AA-CAES. *International Journal of Energy Technology and Policy*, 5:296–306(11), 6 August 2007.
- [8] EPRI and U.S. Department of Energy. EPRI - DOE Handbook of Energy Storage for Transmission and Distribution Applications. Technical report, Electric Power Research Institute, Palo Alto, CA, and the U.S. Department of Energy, Washington, DC, 2003.
- [9] W. F. Pickard, N. J. Hansing, and A. Q. Shen. Can large-scale advanced-adiabatic compressed air energy storage be justified economically in an age of sustainable energy? *Journal of Renewable and Sustainable Energy*, 1(3):033102–1 – 033102–10, 2009.
- [10] G. Grazzini and A. Milazzo. Thermodynamic analysis of CAES/TES systems for renewable energy plants. *Renewable Energy*, 33(9):1998 – 2006, 2008.
- [11] I. Arsie, V. Marano, G. Nappi, and G. Rizzo. A model of a hybrid power plant with wind turbines and compressed air energy storage. *Proc. of ASME Power Conference*, 2005.
- [12] H. Lund, G. Salg, B. Elmegaard, and A. N. Andersen. Optimal operation strategies of compressed air energy storage (CAES) on electricity spot markets with fluctuating prices. *Applied Thermal Engineering*, 29(5-6):799 – 806, 2009.
- [13] L. Nielsen and R. Leithner. Modelling and dynamic simulation of an underground cavern for operation in an innovative compressed air energy storage plant. *5th International Conference on Energy, Environment, Ecosystems and Sustainable Development (EEESD '09)*, 2009.
- [14] European Power Exchange Spot SE. European Power Exchange Market Data 2009. www.epexspot.com/en/market-data.
- [15] D. Laing, D. Lehmann, M. Fiss, and C. Bahl. Test Results of Concrete Thermal Energy Storage for Parabolic Trough Power Plants. *Journal of Solar Energy Engineering*, 131(4):041007, 2009.
- [16] N. Elsner, S. Fischer, and J. Huhn. *Grundlagen der Technischen Thermodynamik, Band 2: Wärmeübertragung*. Akademie Verlag, Berlin, 1993.
- [17] J. Löfberg. Yalmip : A Toolbox for Modeling and Optimization in MATLAB. In *Proceedings of the CACSD Conference*, Taipei, Taiwan, 2004.
- [18] The Mathworks. Optimization Toolbox User's Guide, 2008.
- [19] E. F. Camacho and C. Bordons. *Model Predictive Control*. Springer Verlag, Berlin, 2004.
- [20] J.B. Rawlings. Tutorial Overview of Model Predictive Control. *Control Systems Magazine, IEEE*, 20(3):38 –52, jun. 2000.
- [21] E. D. Sontag. Nonlinear Regulation: The Piecewise Linear Approach. *Automatic Control, IEEE Transactions on*, 26(2):346 – 358, April 1981.
- [22] K. Heussen, S. Koch, A. Ulbig, and G. Andersson. Energy Storage in Power System Operation: The Power Nodes Modeling Framework. Presented at the *IEEE PES Conference on Innovative Smart Grid Technologies Europe*, Gothenburg, Sweden, 2010.
- [23] European Energy Exchange (EEX), Leipzig, Germany. www.eex.com.

Annex

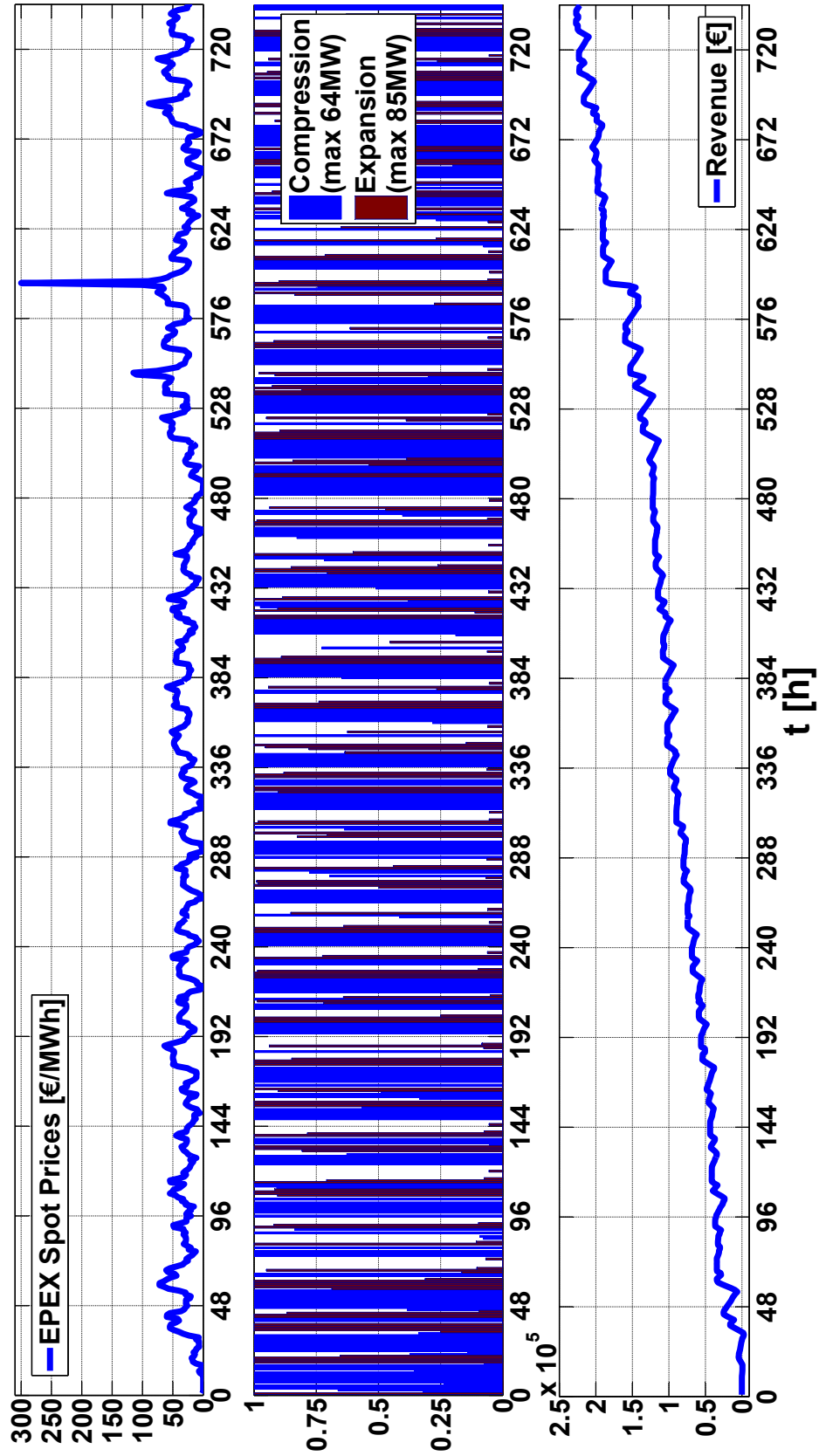


Figure 9: Optimal operation strategy of the AA-CAES model (Simulation time: 1–31 January 2007, $N = 24$ h, initial SOC: 50%).